Trajectory straggling and nonlinear effects in the energy loss of surface-channeled ions

A. Robin,[1] M. Reiniger,[1] A. Närmann,[2] M. Schleberger,[3] J. I. Juaristi,[4] and W. Heiland[1]
[1]*Universität Osnabrück, D-49069 Osnabrück, Germany*
[2]*Detecon Consulting GmbH, D-53227 Bonn, Germany*
[3]*Universität GH Essen, Institut für Experimentelle Physik, D-45117 Essen, Germany*
[4]*Centro Mixto CSIC-UPV/EHU, Facultad de Químicas, Universidad del País Vasco, Apartado 1072, E-20080 San Sebastian, Spain*
(Received 2 August 2002; revised manuscript received 28 January 2003; published 14 April 2003)

We have performed surface-channeling experiments with He^+ ions in the energy range between 0.5 keV and 3.5 keV scattering off a flat Pd(110) surface. The energy-loss spectra are measured by a time-of-flight analysis at grazing incidence for different surface directions. The shape of the energy-loss spectra is found to depend strongly on the azimuthal direction. Along axial channeling directions, the energy spectra are broadened and multipeak structures are found. The analysis of these features allows insight into the inelastic interaction process with the surface electrons, which is found to depend strongly on the projectiles' trajectories. Deviations from a linear dependency of the mean energy loss on the primary energy are observed and partly explained by the introduced surface-channeling model including the analysis of detailed trajectory calculations. The significant broadening of the energy spectra is mainly attributed to trajectory straggling.

DOI: 10.1103/PhysRevB.67.165409 PACS number(s): 61.85.+p, 34.50.Bw, 34.50.Dy, 79.20.Rf

I. INTRODUCTION

Recent ion-surface scattering experiments open new possibilities to investigate the electronic-density profile at surfaces by analyzing the measured energy-loss distributions.[1] The use of grazing scattering conditions ensures that the perpendicular momentum is low enough to prevent particles to penetrate the first atomic layer. Under these conditions one observes surface planar channeling where the surface acts as a mirror, and mainly reflects the scattered particles specularly. As a rough number, the *perpendicular* energy $E_\perp = E_0 \sin^2\psi$ has to be lower than $\sim$30 eV to ensure surface planar channeling conditions. In grazing surface scattering experiments the contribution of nuclear energy transfer to the total energy loss of the projectiles is quite small and can be estimated within a simple binary collision model. Therefore, grazing ion-surface scattering is a well-suited technique to investigate electronic energy losses arising from interactions between the projectiles and the surface electrons.[2–5] These inelastic processes are strongly related to the target electron density.

The theoretical treatment is complicated by the fact that surface scattering in general consists of a large number of individual scattering processes contributing to the total energy loss of the particles. The multitude of elastic collisions with the target atoms causes a significant trajectory variation, called *trajectory straggling*. The influence of this contribution on the energy spectra is usually neglected. Additional spectral broadening features appear when scattering takes place along surface channels, e.g., the $\langle 110 \rangle$ direction. Here, the projectiles are guided by the elastic interaction with the atomic chains. This phenomenon is known as *axial* channeling and causes nonplanar trajectories or out-of-plane scattering events.[6] Additionally, the interaction time with the periodic surface potential is essentially increased under axial channeling conditions as, e.g., is used in resonant coherent excitation experiments.[7–9] Under these conditions, higher inelastic contributions to the total energy loss can be expected due to enhanced interactions with the electron gas.[6]

In this work, we present surface-channeling experiments of He^+ ions scattered off a Pd(110) surface under grazing scattering angles ψ with E_0 varying between 0.5 keV and 3.5 keV. The projectile velocity v is small compared to the *Fermi* velocity $v_F = (3\pi^2 n_0)^{1/3}$. Here, n_0 denotes the target electron density. For these low particle velocities, plasmon excitations can be neglected. Therefore, the production of electron-hole pairs is proposed to be the main energy-loss channel. Theories for the projectile velocities under investigation describe the inelastic losses by the friction of a point charge moving in a free-electron gas.[10–13] Here, the electronic stopping power increases linearly with the projectile velocity v.

Surface scattering experiments in the low-energy range ($v < v_F$) using flat (111) surfaces are hardly affected by the electronic surface corrugation.[2,14] Consequently, the trajectory variation of the projectiles has less influence on the energy-loss distribution and a simple analytical description for a kind of ''average'' trajectory is satisfactory for theoretical treatment.[2] Different dependencies of the energy loss on the particle velocity are found in the literature[2,14] following the relation $\Delta E \sim v^q$ with values for q ranging between 1.7 and 3. These variations of the exponent q are attributed to different stopping-power values, whereas no influence of a variation of the trajectory length with velocity is considered. The importance of considering trajectory length variations depending on scattering parameters such as projectile velocity, angle of incidence, and azimuthal direction has been shown recently for the system N on Pt(110).[1,15] Here, the observed effects are covered by the strong corrugation of the missing-row reconstructed Pt(110) surface. In the work presented here we investigate to the best of our knowledge, trajectory effects on the energy spectra of ions scattered off a noncorrugated surface including trajectory straggling and axial channeling contributions. The trajectory influence as well as the stopping power are investigated in dependence of

the surface direction. The stopping power results are found to differ slightly from former experiments. In order to compare the experimental spectra with calculated spectra, we perform detailed trajectory calculations for the four investigated surface directions, which give detailed insight into the different types and characteristics of surface channeling.

II. THEORETICAL ASPECTS

For the description of the energy loss of charged particles scattering off metal surfaces we have lately proposed a model, which combines trajectory calculations and stopping characteristics of the target,[15] For the system N on Pt(110), the model gave good agreement between theory and experiment over a wide range of primary energies.[1,15] In our calculations, the projectile velocity v is taken as constant during the scattering process and nuclear stopping contributions are neglected. Therefore, the energy loss ΔE is approximated by

$$\Delta E = \frac{dE}{ds}\ L = S_e L, \tag{1}$$

where dE/ds is the inelastic electronic energy loss per unit path length (S_e, stopping power) and L is the interaction length, i.e., the part of the trajectory in which the ion interacts efficiently with the valence electrons of the metal surface.[16–18] The stopping power depends on the particle velocity and on the transport cross section $\sigma_{tr}(v_F)$ at the Fermi level, calculated for electron scattering in the potential induced by the projectile. Here, this potential is calculated using density-functional theory (DFT) for an impurity embedded in an electron gas.[10] Taking a free-electron radius for Pd of $r_s = 1.51$ a.u., which is evaluated from the plasmon peak in electron energy loss[19] spectra, the electronic stopping power for He interacting with Pd is calculated to

$$S_e^{bulk} = \gamma^{bulk}\ v = 0.743 v \text{ a.u.} \tag{2}$$

The parameter γ^{bulk} characterizes the respective *friction coefficient* for the interaction of the He ions with the Pd electrons. The particle velocity v is given in units of the *Bohr* velocity v_0. The trajectory length L in Eq. (1) is computed from a Monte Carlo code. For determining a trajectory length from the calculations we define a surface distance z_{edge}, where the trajectory starts and ends. The parameter z_{edge} limits the interaction distance, i.e., the energy loss for z outside z_{edge} is estimated to be negligibly small, i.e., approximately a few eV.[3] For the evaluation we take only trajectories within the acceptance angle of the detector into account.

The above discussed procedure is applied to every single calculated trajectory giving the energy loss for the respective projectile. By counting the number of projectiles contributing to a certain energy interval $[E_a, E_b]$ with channel width $E_b - E_a$ we are able to calculate histogramlike energy spectra and compare these with the experimental spectra.

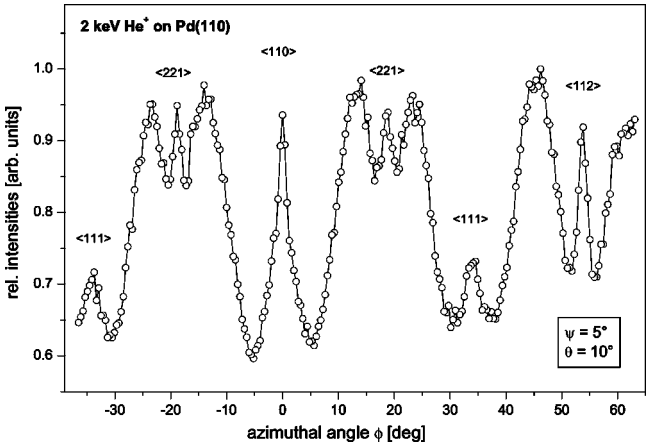

FIG. 1. Azimuthal scan of 2-keV He on Pd(110). Intensity vs azimuthal angle is shown in case of forward scattering geometry. Labels indicate the respective surface directions.

III. EXPERIMENT

The experiments are done in a UHV chamber described in detail elsewhere.[20] Here, only a brief overview of the main experimental features shall be given. The ion beam is produced in a plasma ion source. A 90° sector field magnet performs charge and mass selection. The energy is measured using a pulsed ion beam and a time-of-flight (TOF) system. The TOF system affords an energy resolution $\Delta E/E_0$ of $\approx 10^{-3}$ and has a full width acceptance angle of 1.2°. From other measurements it is known that the detection probability for light particles such as He is ~ 1 for particle energies $E_0 > 1$ keV. Since we find that more than 99% of the particles are neutral after the scattering process, we usually do not separate the scattered charge states by using postacceleration. All measurements are done in specular reflection geometry, i.e., $\theta = 2\psi$ is used. A glancing angle of incidence of $\psi = 5°$ is used in all cases leading to kinetic energies perpendicular to the surface of $E_\perp = 3.4$ eV–27 eV. These values are still in the range of surface channeling.

The target is mounted on a three-axes manipulator and can be heated by electron bombardment. Surface preparation of Pd is done by cycles of 2 keV Ne^+ sputtering under grazing incidence of 8° and consecutive annealing at 300 °C. Surface cleanliness is controlled by ion desorption spectroscopy. This technique analyzes the time of flight of the forward sputtered particles to determine the particle mass according to the binary collision approximation.[21,22] Ion desorption spectroscopy is sensitive to contaminations in the surface layer(s) of ≈1%. Analyzing the ion desorption spectra after surface preparation, we can exclude any surface contamination. The orientation of the target is done measuring the scattering intensity in azimuthal scans. This technique allows an identification of the different surface directions within a precision better than $\Delta\phi = 1°$ (Fig. 1).

IV. RESULTS

The elastic interaction of the ions with the target atoms strongly influences the scattering distribution. Figure 1

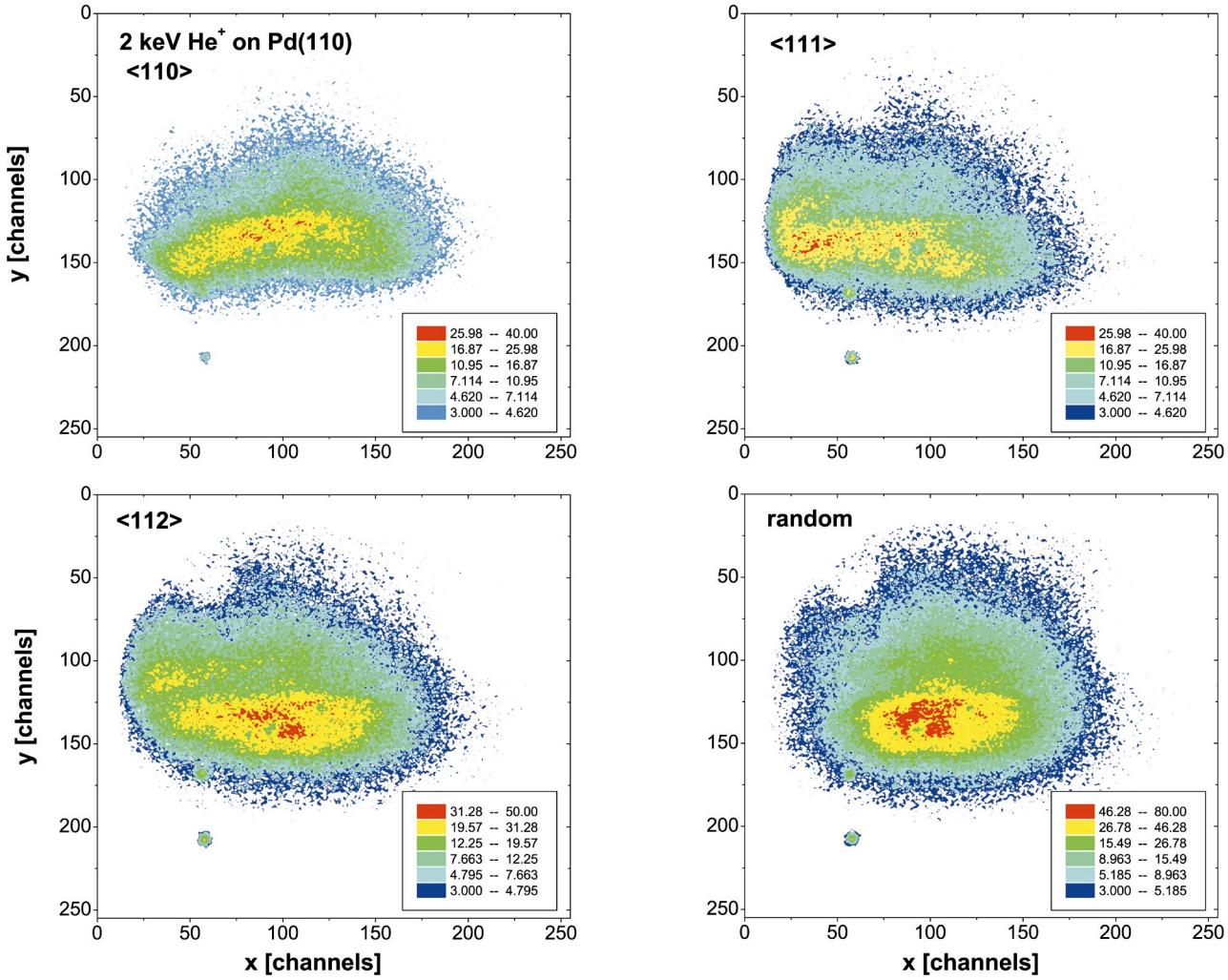

FIG. 2. (Color) Two-dimensional scattering distributions for the $\langle\bar{1}10\rangle$-direction, $\langle 111\rangle$-direction, $\langle 112\rangle$-direction, and a random surface direction, respectively. The x axis indicates the direction of the azimuthal angle, the y axis corresponds to the scattering angle. Spectra are taken with a position sensitive detector (PSD) for 2-keV He on Pd(110) and a fixed angle of incidence of $\psi=5°$. The little spot in the lower left corner is a detector artifact.

shows an azimuthal scan, where the different surface directions can be identified very precisely by maxima in the scattered intensity. A comparison with a spectrum calculated from the MARLOWE program code[23,24] shows reasonable agreement.[25] An overview of the spatial scattering distributions is given by the x-y diagrams in Fig. 2. These two-dimensional scattering distributions are taken with a position sensitive detector. The maximum particle count rate was $I_{max}=5000$ counts/s and, therefore, low enough to avoid data processing problems.

The shape of the distributions is clearly distinguishable for the different azimuthal directions. When scattering along a surface channel a *half-moon* distribution is seen, especially in case of the $\langle 110\rangle$ surface direction. This indicates the strong broadening of the projectile trajectory distribution by axial channeling effects. In case of *random* scattering the scattering distributions appear less broadened and obey roughly Gaussian distributions in both directions. We remember that only a small part of the whole scattering distribution is detected by our small-angle time-of-flight system.

We have taken energy spectra for four different surface directions: $\langle 110\rangle$ with $\phi=0°$, $\langle 111\rangle$ with $\phi=35.3°$, $\langle 112\rangle$ with $\phi=54.7°$, and a *random* direction ($\phi=45°$), respectively. The differences in the peak shape, the peak broadening, and the mean energy value obtained from the peak maximum position are evident in Fig. 3. The energy distributions in case of scattering along the $\langle 110\rangle$ direction show the largest broadening. It is obvious that they consist of at least two contributions. In the low-energy case ($E_0=1460$ eV, upper panel) the peak shapes for the *random* and the $\langle 112\rangle$ direction look very similar: they show small broadening, less energy loss than in the $\langle 110\rangle$ case, and a Gaussian-like distribution. In contrast, the spectrum is more strongly broadened along the $\langle 111\rangle$ direction. The former described characteristics change partly in case of higher projectile energies as shown in the lower panel of Fig. 3 for $E_0=2646$ eV. A second contribution with higher energy loss appears for the $\langle 111\rangle$, the $\langle 112\rangle$, and the *random* direction and is enhanced in case of the $\langle 110\rangle$ channel. This low-energy tail causes a stronger spectral broadening, which is more evident for the $\langle 112\rangle$ direction

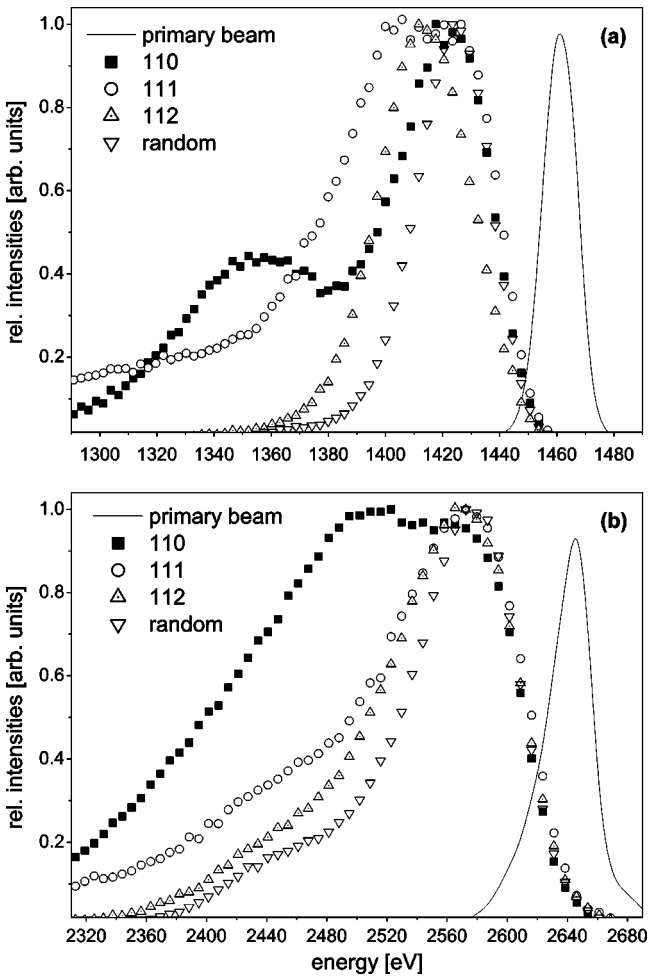

FIG. 3. Experimental energy distributions for He^+ scattered off Pd(110) along four different surface directions. The primary energies are $E_0=1461$ eV (a) and $E_0=2646$ eV (b). The spectra are taken under specular scattering conditions with the angle of incidence fixed to $\psi=5°$.

than for the *random* direction. The spectral features are caused by variations in the trajectory distributions and will be discussed in detail in Sec. V.

As a word of caution, it should be mentioned that the peak shape in the experimental spectra strongly changes already for small variations of the azimuth.[1] This may explain the relative large variations in the measured mean energy-loss values, especially found for scattering along the narrow ⟨111⟩-channel (see Sec. V B).

V. DISCUSSION

We performed detailed trajectory calculations solving Newton's equations of motion to understand the features of the measured energy spectra. Summing up the two-body potentials in a box of $8\times8\times3$ atoms around the actual projectile position we obtain the acting force between surface and projectile. As scattering potential we use the screened Coulomb potential of Ziegler, Biersack, and Littmark with the respective screening length.[26] Thermal vibrations are taken into account within the Debye model using a surface Debye temperature of 190 K to characterize the vibration amplitude perpendicular to the surface.[27]

A. Trajectory straggling

We find specific trajectory distributions for every investigated surface direction. In Fig. 4, typical results are shown for $E_0=1460$ eV. Only trajectories within the acceptance angle of our TOF detection system are selected. The four left panels give a side view showing the depth distribution of the projectiles. The right panels give an on-top view allowing the distinction of *zigzag* channeled particles, referred to as class 2 trajectories, from the *in-row* (class 3) and the *on-top* (class 1) scattered particles. Similar trajectory results calculated with different computer codes for different systems and different surface directions can be found in the literature showing comparable features.[3,15,28]

In case of *random* scattering and along the ⟨111⟩ direction, only one main class of trajectories is found. Here, the axial guiding of the projectiles is low and the particles are channeled mainly *planar on-top* the first layer. However, we find a broadened trajectory distribution in case of the ⟨111⟩-direction (Fig. 4) according to the enhanced broadening in the measured energy spectra found for this direction [Fig. 5(b)]. All in all, the calculated scattering distributions are in reasonable agreement with the experimental distributions presented in Fig. 2.

Apparently, at least two classes of trajectories exist for the ⟨110⟩ channel. They stem from particles scattering *on-top* off the first layer atoms (class 1) and from particles guided *in-row* between the surface channels. A closer look lets us differentiate the latter in particles scattering with only small sidewall interactions (class 3) and particles performing so-called *zigzag* trajectories (class 2). The *zigzag* scattered particles interact with the channel walls, but do not penetrate the first layer (cf. Fig. 4, bottom panels). Due to these three different contributions, the trajectory straggling is enhanced causing the strong broadening found in the energy spectra. Even if the trajectory calculations may not reproduce the scattered intensities for the different peaks exactly, especially in case of the deep ⟨110⟩ channel,[1] we are able to reproduce the basic features of the measured energy spectra including a significant spectral broadening.

Detailed calculations varying the azimuthal angle within small steps around the ⟨110⟩-surface direction show strong effects in the characteristics of the *zigzag* trajectories. Trajectories with *zigzag* character are also observed in case of the ⟨112⟩ direction. Here, the particles start to penetrate the surface layer for energies $E_0\gtrsim2$ keV following rather long trajectories. Therefore, the broadening of the ⟨112⟩ spectra in case of higher E_0 seems to be caused by those particles which penetrate the first layer. These penetrating particles represent an additional class of *zigzag* trajectories. In general, path length and scattering depth of *zigzag* trajectories change strongly with small azimuthal variations. Thus the theoretical description of *zigzag* scattered particles is quite complicated, as could be shown earlier.[1] Therefore, we concentrate in the following on the evaluation of energy-loss values for the class 1 (present in all directions) and the class 3 trajectories (present only in the ⟨110⟩ direction).

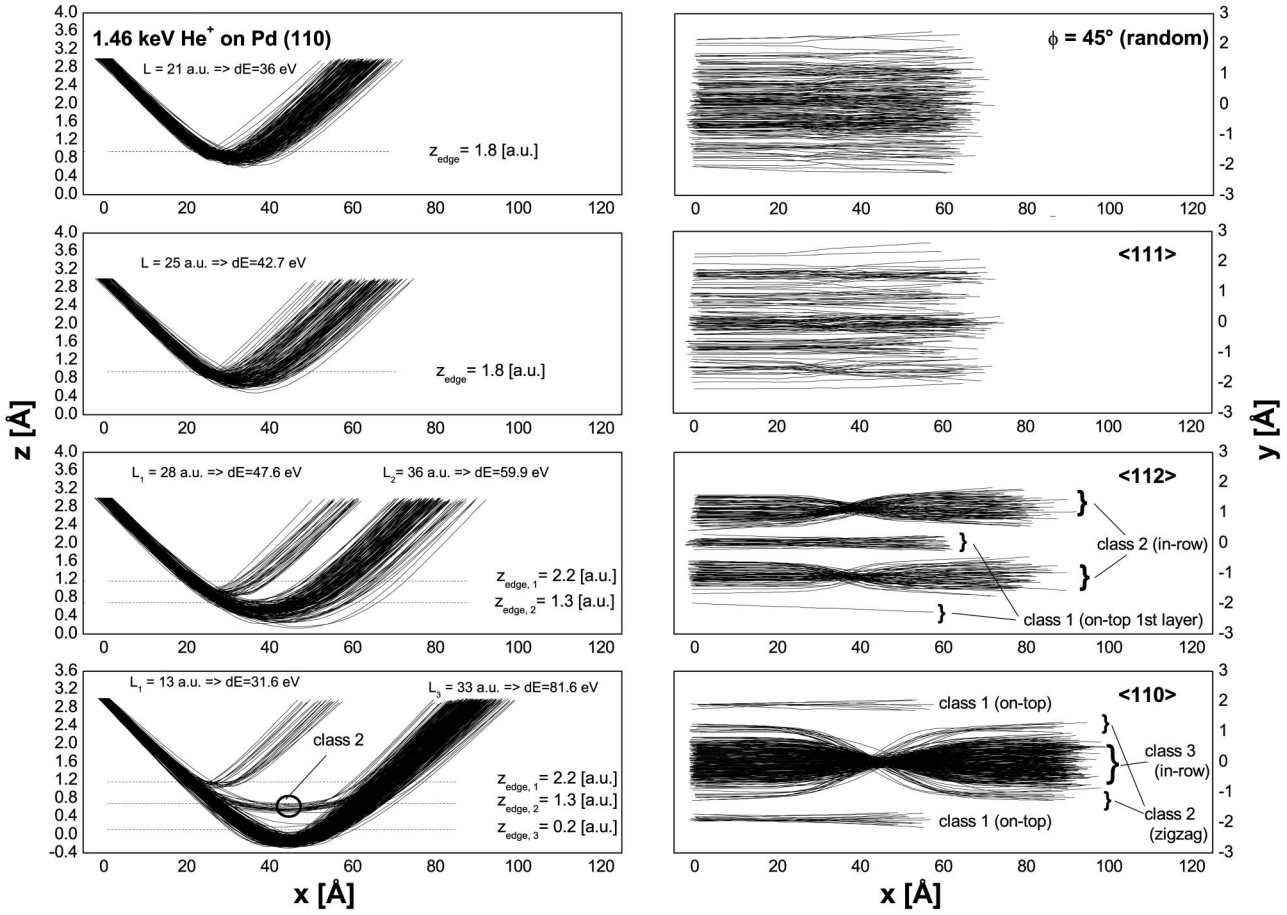

FIG. 4. Calculated trajectories in case of $E_0 = 1460$ eV for the discussed four surface directions. Only particles within the acceptance of the detector are taken into account. Left panels show the depth distribution in a side view, with z giving the distance with respect to the surface plane. Right panels give an on-top view to distinguish the different trajectory classes as indicated. Additionally, calculated average trajectory lengths and energy losses for the indicated z_{edge} values are given (cf. text). Note, the values for z_{edge} are given in atomic units, the axis scales are in angstrom.

B. Energy-loss calculations

We investigate first the *random* direction where, according to the results of Sec. V A, pure planar channeling can be assumed. In a straightforward approach we set the friction coefficient to the calculated bulk value $\gamma^{bulk} = 0.743$ a.u. [Eq. (2)] and adjust the effective interaction range to $z_{edge} \simeq 1.5$ a.u. This procedure has been successfully applied in former studies for the interaction of N with Pt.[15] But in case of He on Pd the agreement between theory and experiment is not satisfactory. Generally, speaking, using γ^{bulk} we find that the calculated energy-loss values increase stronger with E_0 than found in the experiment. Therefore, we use a reduced stopping power. Good agreement with the experiment is obtained with $\gamma = 0.683 \times \gamma^{bulk}$ resulting in $z_{edge} = 1.8$ a.u. as interaction distance [cf. Fig. 6(a)]. The interaction distance of 1.8 a.u. used in the theoretical model corresponds to $\approx$70% of the interplanar distance between the Pd layers. Therefore, the obtained interaction distance slightly exceeds the jellium edge which is defined as half the interplanar distance. But it is smaller than found for planar channeling of N on Pt, where an effective interaction zone of $z_{edge}^{\mathrm{Pt}} = 2.6$ a.u. leads to satisfactory results for keV up to MeV ion energies.[1,15] The adjusted stopping power for the system He-Pd is $\sim$30% lower than calculated from DFT and approximately by a factor of 3 smaller than the stopping power obtained for the system N-Pt. The observed deviations from the results for N on Pt are attributed to both, different electron-density distributions at the surfaces as well as to different electronic properties of the projectiles. From many experimental and theoretical work it is known that the stopping power oscillates with the atomic number Z_1 of the projectile.[10,18,29,30] One finds that the stopping power reaches maximum for values of Z_1 between 5 and 8. The Z_1 oscillations are to a wide extent responsible for the large stopping-power difference between He and N and support our empirical estimation for $\gamma^{\mathrm{He}\rightarrow\mathrm{Pd}}$. The smaller z_{edge} value in case of Pd is probably due to the higher electron density compared to Pt [$r_s^{\mathrm{Pd}} = 1.51$ a.u. vs $r_s^{\mathrm{Pt}} = 1.63$ a.u.] (Ref. 15). A higher bulk electron density causes a steeper decrease of the electron density in the region of the jellium edge. The relative electron density for surface distances exceeding the jellium edge is therefore lower[31–33] in case of Pd, and the effective interaction zone is reduced.

The parameters used for the *random* direction give reasonable results for the $\langle 111 \rangle$-direction, too. Good agreement

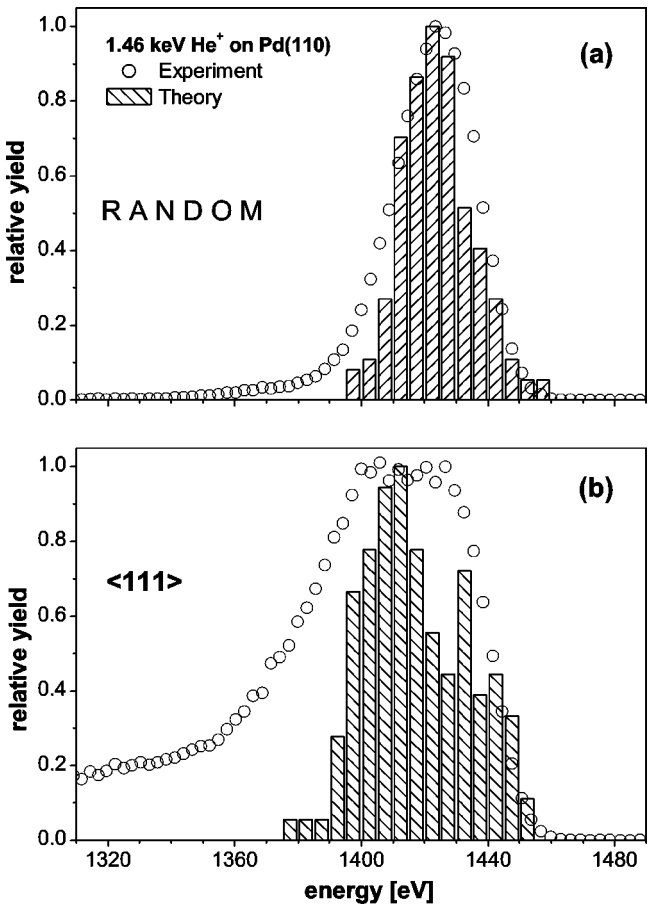

FIG. 5. Comparison of experimental and calculated energy distributions for the *random* (a) and the ⟨111⟩ direction (b), respectively. The primary energy is taken as 1460 eV in all cases. For the theoretical calculations $z_{edge}=1.8$ a.u. and $\gamma=0.508$ a.u. are used.

is achieved for energies down to $E_0=750$ eV, as shown in Fig. 6(b). A further lowering of E_0 causes the model to fail. This is intrinsic to the model since a minimum perpendicular momentum is needed allowing the particles to penetrate the interaction zone, which is defined by z_{edge}. However, for energies $E_0>2500$ eV the theoretical model overestimates the experimental energy-loss values. We suggest the following aspects to be responsible for this behavior:

(i) Since the ⟨111⟩ channel is relatively narrow, we might not hit the channel exactly in all cases. In that case, we can expect lowered experimental energy losses, which are comparable with the values found for the *random* direction. With this assumption we can also explain the relatively large variation of the experimental losses in contrast to the results for other directions.

(ii) The trajectory calculations show particles penetrating the first layer in case of higher primary energies. The contribution of these particles may be overestimated by the calculations because surface structure effects like steps prevent the projectiles from following these trajectories.

(iii) As shown in Fig. 4, the trajectory distribution is broadened compared to the *random* case. Due to this enhanced trajectory straggling, the experimental increase of the spectral width is caused [Fig. 5(b)]. This effect enhances as well the statistical uncertainty in our theoretical model.

Summarizing the results obtained for the ⟨111⟩-surface channel, we find that our model gives reasonable agreement with the experiment. Small deviations are due to trajectory variations in and close by the channel.

The results for the ⟨112⟩ direction are somehow different. The measured energy losses for the ⟨112⟩ direction lie in between the ones for the *random* direction and the ones for the ⟨111⟩ channel [Fig. 6(c)]. The peak shape for energies up to 2000 eV corresponds to the one for the *random* direction, i.e., we can in principle assume planar surface channeling for most of the scattered particles. This assumption is supported by the trajectories of the particles showing only a small length and depth variation. But in principle, we deal already at low energies with two trajectory classes, the *on-top* scattered ions, which result in the main contribution of the energy spectra, and the ions with higher energy losses which travel *in-row* the channels. Expanding the interaction zone for the *on-top* channeled particles to $z_{edge}=2.2$ a.u., we get an excellent agreement with the experimental data. The modification of the z_{edge} value accounts for the different channel characteristics. The distance between next-neighbor atoms inside the atomic string of the ⟨112⟩ channel is smaller by a factor of $\sqrt{2}$ compared to the ⟨111⟩ direction. This enhances the surface potential along the ⟨112⟩ direction and causes the trajectory turning points of the nonpenetrating on-top scattered particles to be further away from the surface than in case of the ⟨111⟩ channels (cf. Fig. 4). Additionally, as known from low-energy ion spectroscopy, ⟨112⟩ channels are broader than ⟨111⟩ channels,[34] causing an enhanced depth spreading of the trajectories, and allowing the particles to penetrate the surface more easily. As a result, we observe more and more particles penetrating the surface layer when increasing the primary energy above a certain threshold of $\approx$2 keV, corresponding to $E_{\perp}\simeq 15$ eV. But, these particles do not contribute to the main peak in the energy spectrum and are therefore neglected in the calculations shown in Fig. 6(c). Here, only the *on-top* scattered particles (class 1) are included.

The results for scattering along the ⟨$1\bar{1}0$⟩ direction [Fig. 6(d)] are strongly influenced by the enhanced surface corrugation present for this channel. The surface corrugation causes a splitting of the trajectories in different classes with different scattering characteristics (Fig. 4, bottom panels). A detailed discussion of these effects follows in Sec. V D. Summarizing our energy-loss results at this point we find that our model calculations describe the dependency on the primary energy reasonably for the discussed surface directions. The theoretical predictions for the stopping power which are based on the model of a point charge perturbing a free-electron gas, and thus neglecting the spatial electron distribution of the projectile and at the surface, lead to small, but significant deviations from the experiment.

C. Energy broadening

Penetration of particles through the surface layer increases significantly the energy loss. Therefore, surface pen-

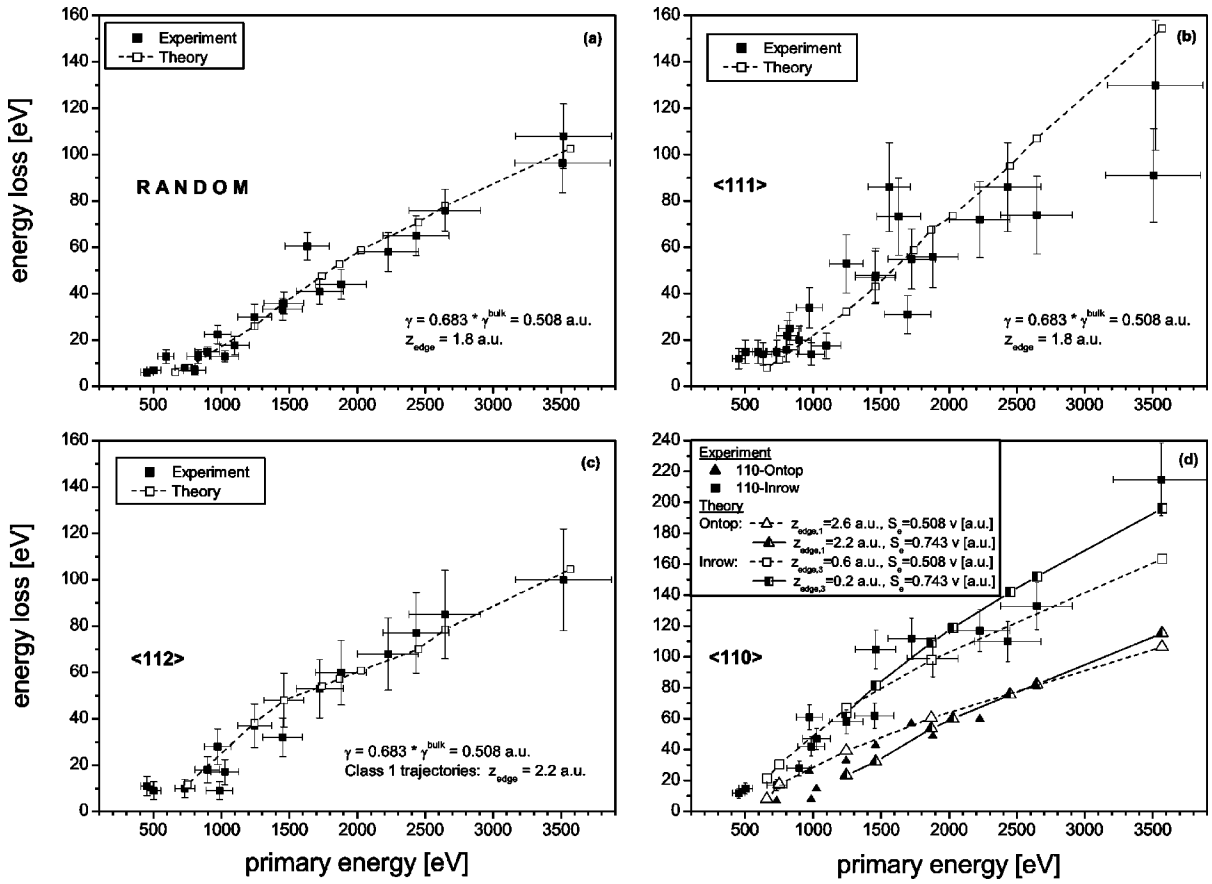

FIG. 6. Comparison of experimental and theoretical mean energy losses for four different surface directions [(a)–(d)] in case of ψ=5° and θ=10°. In case of the ⟨110⟩ direction, the theoretical values are evaluated for two different parameter sets (S_e,z_{edge}), and the energy losses are calculated separately for *on-top* and *in-row* channeled particles, respectively.

etration of parts of the projectiles results in enhanced energy broadening. In case of the ⟨110⟩ channel we observe long *in-row* trajectories from very low projectile energies on (Fig. 4, lowest panels). These *in-row* and *zigzag* channeled particles follow all hyperboliclike curves in the *x*-*z* plane, and their path lengths exceed the one for *on-top* channeled particles by a factor of 2 or 3. Consequently, these particles will suffer enlarged energy losses leading to the observed low-energy shoulder and to a significant broadening in the energy spectra (see Fig. 3).

For the ⟨112⟩ direction, penetration is observed for higher energies only because the ⟨112⟩-channel width restricts penetration through the first layer to higher projectile velocities, corresponding to perpendicular energies $E_\perp$ which exceed ~15 eV. The penetrating projectiles interact strongly with the channel sidewalls and are guided a long path beneath the first surface layer (Fig. 7). However, no sideward change of the surface channel is observed. The penetrating particles perform *hyper*-channeling with many sidewall reflections. These hyperchanneled particles define a new class of trajectories following ''special'' *zigzag* trajectories (see Fig. 7). These particles pass a subsurface channel over large distances with an approximately constant *z* value and relatively large impact parameters. Path lengths can exceed the one for *on-top* channeled particles by a factor of 5 or 6. For these subsurface channeled particles an accurate theoretical prediction of the energy loss is difficult to obtain. A complete energy distribution calculated for slow (1.4 keV) ions scattering along the ⟨112⟩ channel is given in Fig. 8(a) and compared with the experiment. It shows good agreement using two sets of

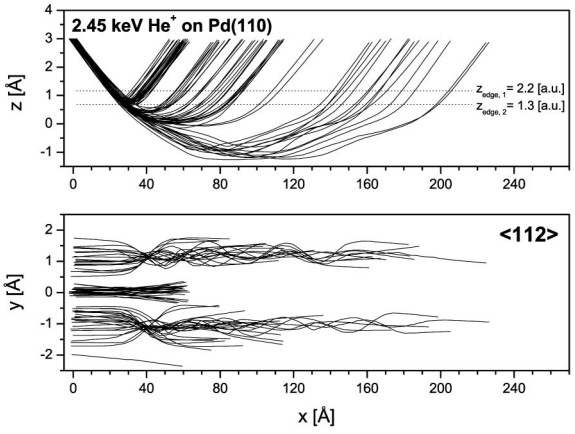

FIG. 7. Side and top view of trajectories calculated for 2.45-keV He ions scattering along the ⟨112⟩ channel. Trajectories penetrating the surface layer and performing hyperchanneling are shown at position $y \simeq \pm 1$ Å in the lower panel. The short trajectories at $y \simeq 0$ Å and $y \simeq -2$ Å result from scattering off the ridge surface atoms.

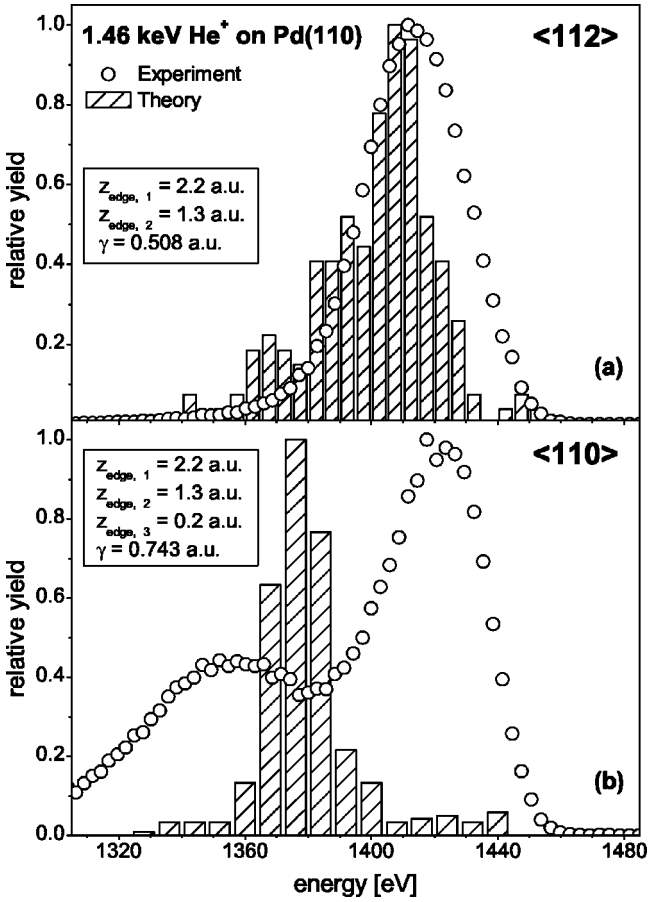

FIG. 8. Comparison of experimental and calculated energy distributions for the ⟨112⟩ direction (a) and the ⟨110⟩ direction (b), respectively. The primary energy is taken as 1460 eV in all cases. Labels indicate the respective model parameters used in the calculation.

model parameters (γ, z_{edge}) for the two trajectory classes. For the projectiles following the class 1 trajectories we extend the interaction zone to $z_{edge,1}=2.2$ a.u. (Fig. 4). For the class 2 trajectories we choose $z_{edge,2}=1.3$ a.u. as interaction zone. The friction coefficient stays $\gamma=0.508$ a.u. for both classes. With these parameters, even the energy broadening is well reproduced indicating a nice agreement between calculated and experimentally found intensities for the different trajectory classes. From this result we conclude that the contribution from different particle trajectories has a very important effect on the broadening of the energy distribution. We find that the energy broadening caused by trajectory straggling is of the order of 30 eV–40 eV, and therefore has the same order of magnitude as the broadening due to electronic straggling, e.g., originating from charge-exchange processes.[3]

D. Surface corrugation

From the experimental spectra, we evaluate both mean peak positions observed in case of the ⟨110⟩ channel, and we plot them against E_0 as shown in Fig. 6(d). Roughly speaking, *in-row* channeling (low-energy peak) results in double the energy loss as *on-top* and *random*, i.e., planar scattering. To describe both contributions within our theoretical model, we replace the planar by a corrugated surface similar to what has been done in case of N on Pt.[1] Three z_{edge} values corresponding to the three trajectory classes are introduced. $z^{110}_{edge,1}$ describes the interaction zone of the *on-top* particles, the second parameter at $z^{110}_{edge,2}=1.3$ a.u. separates the long *zig-zag* trajectories from the deeper penetrating *in-row* particles, described by $z^{110}_{edge,3}$. However, it turns out that a straightforward determination of proper values for the parameters γ, $z^{110}_{edge,1}$, and $z^{110}_{edge,3}$ is difficult.

Figure 6(d) shows the results for two different sets of parameters fitting the experimental values within a good agreement. Increasing the interaction zone for *on-top* channeled particles to $z^{110}_{edge,1}=2.6$ a.u. and for *in-row* channeled particles to $z^{110}_{edge,3}=0.6$ a.u while applying the reduced stopping power value as used for the other surface directions, we are able us to evaluate energy-loss values for primary energies down to $E_0 = 750$ eV. The agreement with the experimental values is reasonable, though the slopes of both calculated graphs (for the *on-top* and the *in-row* contribution, respectively) are slightly weaker than in the experiment. By increasing the stopping-power value up to S_e^{bulk} we get a better agreement with respect to the slope of the graphs, but we have to adapt the interaction zone by using lower z_{edge}-values, i.e., 2.2 a.u. for the *on-top* trajectories and 0.2 a.u. for the *in-row* scattered particles as indicated in Fig. 6(d). The latter set of parameters, however, limits the applicability of the model to perpendicular energies which fulfill $E_\perp \gtrsim 10$ eV, corresponding to $E_0 \gtrsim 1.3$ keV in case of $\psi=5°$.

We compare the calculated energy distributions with the experimental spectra in Fig. 8(b) for $E_0=1460$ eV. The experimentally observed broadening is much larger than the calculated one. This effect might be caused by a significant overestimation of the intensity for the *in-row* scattered particles in the calculations. In fact, the experiment shows the *on-top* contribution to dominate.

A comparison of the experimental peak shapes observed for the ⟨110⟩-surface direction with the one found for[1] N on Pt shows a clear change in the intensities of the two contributing peaks, which are attributed to the *on-top* and *in-row* scattered particles, respectively. For He on Pd the intensity of the *on-top* scattered particles seems to exceed over the intensity of the *in-row* trajectories. For N on Pt(110), however, it was found to be vice versa. As an explanation for this finding, we remind the reader that Pt(110) forms a (1×2) surface reconstruction, the so-called *missing-row* surface structure.[35] That means, every second atomic chain along the ⟨110⟩ direction is missing in the surface layer resulting in an enhanced electronic corrugation. The probability for trajectories to scatter along these deep *in-row* channels is considerably higher than for the Pd surface and the projectiles can easily penetrate the first layer.

E. Nonlinear effects

As can be concluded from Fig. 6 the presented energy-loss measurements do not show a straight linear dependency of the mean energy loss with the primary energy. In case of

the ⟨112⟩-direction, an energy-dependent slope for the increase of the energy loss with E_0 is evident from the experiment. This may be assumed for the ⟨110⟩ and the ⟨111⟩ direction as well, even though the experimental uncertainties are higher in these cases.

From the results of the trajectory calculations we find that the increase of the average trajectory length with E_0 is not linear, but depends strongly on the projectile energy and the surface direction. The increase of the average trajectory length with primary energy basically gets smaller if the perpendicular energy exceeds 10 eV–12 eV. This observation explains the experimentally found deviation from a linear dependency of the energy loss on the particle energy (see Fig. 6). Furthermore, the observed trajectory straggling affects significantly the mean energy loss. This strong influence of the trajectory straggling on the energy spectra has not been reported up to now. Usually, it is assumed that electronic effects such as charge exchange and plasmon excitation mainly cause the spectral energy broadening.

Another deviation from linearity is found for all surface directions under investigation, namely, a minimum energy-loss value of $\Delta E_2 \sim 10$ eV for E_0 between 450 eV and 750 eV, which seems not to decrease further. This is in contrast to the predictions of the linear theory.[10–12] Therefore, an additional energy loss channel with a different stopping dependency is supposedly active in case of low projectile velocities and small values of $E_\perp$. Stölzle and Pfandzelter discuss such an intercept in the energy loss of protons scattering off a graphite surface with medium primary energies.[36] They find $\Delta E_2 = \Delta E_2(E_\perp)$ and attribute ΔE_2 to charge-exchange processes during the interaction, even if the outgoing charge state is neutral. Indeed, according to the binary collision model the nuclear losses are much too small to explain this effect, since they are of the order of $\leqslant 1$ eV. The same holds for the experimental uncertainties caused by calibration errors, which are expected not to exceed the order of 5 eV. Therefore, ΔE_2 cannot be completely explained by one of those effects.

For a more accurate description, contributions from other effects such as the image potential[37] and far distance effects of the *Coulomb* interaction[3] have to be included, which can affect the energy loss additionally by a few eV. We assume that the measured intercept is caused by the sum of all the aforementioned effects resulting in a significant experimental deviation from the linear dependency in case of very small projectile velocities.

VI. CONCLUSION

We investigated the energy-loss dependency on E_0 for different azimuthal directions in case of singly charged He ions scattering off Pd(110). Looking in detail, we find deviations from the well-known linear dependency. These deviations can be basically explained by results from trajectory calculations. In fact, axial channeling effects play a major role for the ⟨110⟩ channel. Here, first layer penetration is already observed for low energies and in addition *zigzag* trajectories lead to an enhanced broadening of the spectra. In a less strict sense, these results hold as well for the hyperchanneled particles found in case of the ⟨112⟩ channel when using perpendicular energies $E_\perp \gtrsim 15$ eV. For $E_\perp < 15$ eV the axial channeling effects are comparatively small for all channels except for the ⟨110⟩ channel. In general, we find the energy spectra significantly broadened due to trajectory straggling effects, especially in case of the ⟨111⟩ direction.

We applied the introduced energy-loss model successfully to all azimuthal directions under investigation with the limitation that $E_\perp \gtrsim 5$–6 eV has to be fulfilled. The stopping-power values used in the model are reasonable, since they are between 70% and 100% of the theoretical value calculated for the He-Pd system. We assume that deviations from the theoretical stopping-power values are related to the projectile size as well as to different screening characteristics, e.g., compared to nitrogen, having an influence on both model parameters, the friction coefficient γ as well as the depth of the interaction zone represented by z_{edge}.

ACKNOWLEDGMENTS

We thank A. Arnau and R. Morgenstern for many fruitful discussions. Financial support from the Deutsche Forschungsgemeinschaft (DFG) is gratefully acknowledged. A.R. is grateful for financial support from the Max-Planck-Preis of P. M. Echenique during the time spent in San Sebastian. J.I.J. acknowledges partial financial support by UPV/EHU, Eusko Jaurlaritza and the Spanish DGICYT (Grant No. BFM2001-0076).

[1] A. Robin, J. Jensen, D. Ostermann, and W. Heiland, Nucl. Instrum. Methods Phys. Res. B **193**, 573 (2002).
[2] C. Auth, A. Mertens, and H. Winter, Nucl. Instrum. Methods Phys. Res. B **135**, 302 (1998).
[3] A. Närmann, W. Heiland, R. Monreal, F. Flores, and P.M. Echenique, Phys. Rev. B **44**, 2003 (1991).
[4] A. Närmann, R. Monreal, P.M. Echenique, F. Flores, W. Heiland, and S. Schubert, Phys. Rev. Lett. **64**, 1601 (1990).
[5] J. Limburg, C. Bos, T. Schlathölter, R. Hoekstra, R. Morgenstern, S. Hausmann, W. Heiland, and A. Närmann, Surf. Sci. **409**, 541 (1998).
[6] A. Robin, N. Hatke, A. Närmann, M. Grether, D. Plachke, J. Jensen, and W. Heiland, Nucl. Instrum. Methods Phys. Res. B **164-165**, 566 (2000).
[7] K. Kimura, H. Ida, M. Fritz, and M. Mannami, Phys. Rev. Lett. **76**, 3850 (1996).
[8] N. Hatke, M. Dirska, M. Grether, E. Luderer, A. Robin, A. Närmann, and W. Heiland, Phys. Rev. Lett. **79**, 3395 (1997).
[9] C. Auth, A. Mertens, H. Winter, A.G. Borisov, and F.J.G. de Abajo, Phys. Rev. Lett. **79**, 4477 (1997).
[10] P.M. Echenique, R.M. Nieminen, J.C. Ashley, and R.H. Ritchie, Phys. Rev. A **33**, 897 (1986).
[11] J. Lindhard and M. Scharff, Phys. Rev. **124**, 128 (1961).
[12] R. Núñez, P.M. Echenique, and R.H. Ritchie, J. Phys. C **13**, 4229 (1980).
[13] M. Kato and Y.H. Ohtsuki, Phys. Status Solidi B **133**, 267 (1986).

[14] A. Närmann, K. Schmidt, W. Heiland, R. Monreal, F. Flores, and P.M. Echenique, Nucl. Instrum. Methods Phys. Res. B **48**, 378 (1990).
[15] A. Robin, W. Heiland, J. Jensen, J.I. Juaristi, and A. Arnau, Phys. Rev. A **64**, 052901 (2001).
[16] J.I. Juaristi, A. Arnau, P.M. Echenique, C. Auth, and H. Winter, Phys. Rev. Lett. **82**, 1048 (1999).
[17] J.I. Juaristi, A. Arnau, P.M. Echenique, C. Auth, and H. Winter, Nucl. Instrum. Methods Phys. Res. B **157**, 87 (1999).
[18] J.I. Juaristi, C. Auth, H. Winter, A. Arnau, K. Eder, D. Semrad, F. Aumayr, P. Bauer, and P.M. Echenique, Phys. Rev. Lett. **84**, 2124 (2000).
[19] C.C. Ahn, O.L. Krivanek, R.P. Burgner, M.M. Disko, and P.R. Swann, *A Reference Guide of Electron Energy-Loss Spectra Covering all Stable Elements* (ASU, HREM Facility, Sun Cities, AZ, 1983).
[20] B. Willerding, H. Steininger, K.J. Snowdon, and W. Heiland, Nucl. Instrum. Methods Phys. Res. B **2**, 453 (1984).
[21] D.P. Smith, Surf. Sci. **25**, 171 (1971).
[22] W. Heiland, H.G. Schäffler, and E. Taglauer, Surf. Sci. **35**, 381 (1973).
[23] M.T. Robinson and O.S. Oen, Appl. Phys. Lett. **2**, 30 (1963).
[24] M. Robinson and I. Torrens, Phys. Rev. B **9**, 5008 (1974).
[25] A. Närmann, Ph.D. thesis, Universität Osnabrück (1989).
[26] J.F. Ziegler, J.P. Biersack, and U. Littmark (Pergamon, New York, 1985), Vol. 1.
[27] D.P. Jackson, Surf. Sci. **43**, 431 (1974).
[28] M. Richard-Viard, S. Abidi, C. Bénazeth, P. Benoit-Cattin, and P. Cafarelli, Nucl. Instrum. Methods Phys. Res. B **184**, 490 (2001).
[29] M.J. Puska and R.M. Nieminen, Phys. Rev. B **27**, 6121 (1983).
[30] I. Nagy, A. Arnau, and P.M. Echenique, Phys. Rev. A **40**, 987 (1989).
[31] C. Höfner, A. Närmann, and W. Heiland, Nucl. Instrum. Methods Phys. Res. B **93**, 113 (1994).
[32] N.D. Lang and W. Kohn, Phys. Rev. B **16**, 4555 (1970).
[33] N.D. Lang, Solid State Phys. **28**, 225 (1973).
[34] H. Derks, Ph.D. thesis, Universität Osnabrück, 1990.
[35] S. Speller, J. Kuntze, T. Rauch, J. Bömermann, M. Huck, M. Aschoff, and W. Heiland, Surf. Sci. **366**, 251 (1996).
[36] F. Stölzle and R. Pfandzelter, Europhys. Lett. **20**, 369 (1992).
[37] U. Kentsch, H. Tyrroff, G. Zschornack, and W. Möller, Phys. Rev. Lett. **87**, 105504 (2001).